LAWRENCE
LIVERMORE
NATIONAL
LABORATORY

LLNL-JRNL-854056

UV-assisted direct ink writing of optically transparent fused silica glass

R. L. Walton, N. A. Dudukovic, J. Johnson, T. D. Yee, D. T. Nguyen, M. Ellis, D. H. Porcincula, C. C. Krikorian, E. B. Duoss, R. Dylla-Spears

September 8, 2023

Advanced Materials Technologies

Disclaimer

ADVANCED MATERIALS TECHNOLOGIES
www.advmattechnol.de

Unlocking Larger Scales and Aspect Ratios in 3D Printed Glass: Coupling Active Mixing and UV Curing for Advanced Printability and Crack Resistance

Beck L. Walton, Nikola A. Dudukovic, Jason Johnson, Timothy D. Yee, Du T. Nguyen, Megan E. Ellis, Dominique H. Porcincula, Caitlyn C. Krikorian, Eric B. Duoss, and Rebecca J. Dylla-Spears*

Recent developments in additive manufacturing (AM) of glass via silica-filled inks have facilitated fabrication of previously unattainable geometries and compositions. However, the maximum processable size of 15 mm limits the use of these prints in applications such as optics. A key limitation lies in the trade-off between material printability and green strength: increasing silica content in the feedstock improves crack resistance and reduces shrinkage but results in dramatic changes in viscoelastic properties that hinder flowability. This paper presents a novel approach that offers expanded versatility in processable size, feedstock formulation, and printing. Described here is a direct ink writing (DIW) system coupled with an active high-shear micromixer and UV light source, capable of simultaneously printing multiple inks with a wide range of rheological properties. Choice of silica sourc, solvent, UV-curable binder, and dispersant is used to tune the ink rheology and improve printability and mechanical properties. Imparting high shear with the micromixer while UV-curing the extrudate allows for increased ink viscosities and reduced nozzle diameters, enabling printing finer feature sizes. With these advances, thin-walled high-aspect ratio structures and a crack-free glass disk measuring 44 mm in diameter are demonstrated, an increase of 3× in the greatest dimension compared to current state-of-the-art.

1. Introduction

The development of glass additive manufacturing (AM) in recent years has helped facilitate advances in near-net shape and multi-material glass forms. AM of glass can be accomplished through direct methods, such as melting glass rods or powders,[1] or indirect methods, such as stereolithography,[2–4] volumetric additive manufacturing,[5,6] 2-photon polymerization,[7,8] or direct ink writing (DIW) of silica-loaded feedstocks, which are subsequently thermally treated to produce glass.[9–13] In particular, glass DIW has been used to fabricate gradient refractive index (GRIN) lenses for advanced optics,[9,10,12] but can also be used to produce lightweight glass structures and near net shape custom optics in one forming step rather than machining a solid piece of material or adhering multiple layers to one another.[14,15] DIW is a promising approach for this application due to the relative ease of printing two or more different materials, as well as the capability to mix inks in-line to create a smooth compositional gradient.

Originally referred to as "robocasting", DIW was first used for fabrication of ceramic materials, such as alumina and zirconia.[16,17] The technique has since come to encompass multiple systems including silicones, metals, magnets, glass, and more.[18] DIW of particle-laden inks requires careful control of ink rheology via particle loading and organic or inorganic additives. Typically, DIW inks are viscoelastic yield stress fluids (YSFs). They exhibit solid-like behavior at rest (allowing shape retention of printed objects), flow at shear stresses exceeding a critical yield point (allowing extrusion), and fast elastic recovery upon cessation of shear (allowing layer-by-layer deposition of filaments). While YSFs do not possess a measurable zero-shear viscosity, their linear elastic shear moduli (G') typically range from 10^4 to 10^5 Pa. Their viscosity during extrusion will depend on the characteristic shear rate, which is a function of the nozzle diameter and the flow rate, typically on the order of 10–100 s^{-1} for nozzles with diameters measuring hundreds of micrometers. The goal in DIW ink formulation is often to maximize the solids loading while without significantly increasing ink viscosity, which is highly sensitive to the particle size and volume fraction. Larger particles can be added at higher volume fractions, while concentrations of smaller particles with much higher surface areas are limited, as the elastic modulus scales with the particle size as $G' \sim a^{-3}$.[11,19] For

B. L. Walton, N. A. Dudukovic, T. D. Yee, D. T. Nguyen, M. E. Ellis, D. H. Porcincula, C. C. Krikorian, E. B. Duoss, R. J. Dylla-Spears
Lawrence Livermore National Laboratory
7000 East Ave, Livermore, CA 94550, USA
E-mail: walton17@llnl.gov
J. Johnson
Purdue University
610 Purdue Mall, West Lafayette, IN 47907, USA

The ORCID identification number(s) for the author(s) of this article can be found under https://doi.org/10.1002/admt.202401284

DOI: 10.1002/admt.202401284

example, early work in DIW of ceramics such as alumina and zirconia used aqueous inks containing 50 vol% ceramic powders with an average particle size of ≈1 μm, which were then sintered to 98% density ceramics.[16,17] However, producing final materials that are optically transparent (i.e., ≈100% density) requires inks with significantly smaller particles to achieve full consolidation.

The first demonstrations of indirect 3D printing of transparent glass were reported in 2017. Kotz et al. used stereolithography of a silica-loaded acrylate resin to produce glass parts up to 15 mm in diameter with feature sizes of ≈80 μm after sintering shrinkage.[2] Nguyen et al. demonstrated DIW of transparent glass using dispersions of fumed silica in tetraglyme (tetraethylene glycol dimethyl ether) as the ink.[9] Since then, DIW of silica and various doped silica glasses has been further developed with both particle-based inks and organic precursor inks, however, scaling these prints >15 mm remains a challenge.[10–13]

While both particle-based and organic precursor inks can produce optical-quality glass, there are important differences in their formulation that have major effects on their post-processing. Particle-based systems include dispersions of fumed silica and/or sol–gel methods which contain precipitated silica nanoparticles, while precursor systems typically include siloxane-based moieties, such as such as polyoctahedral silsesquioxanes (POSS) or polydimethylsiloxane (PDMS),[8] which will convert to SiO_2 upon thermal processing. Generally, for prints in excess of 1 cm as-printed, a particle-based approach is preferred as organic precursor inks can experience large amounts of shrinkage during thermal processing, leading to cracking and failure. Precursor inks, in contrast, are well-suited to small, finely detailed prints, but are generally limited to micron and sub-micron scale parts due to limitations in the diffusion length the organic species must travel to escape the print and the distance silicon atoms must diffuse to coalesce.[8] Both approaches also allow for tailoring the optical properties of the glass by incorporating dopants such as gold, titania, germania, etc. into the ink.[2,3,9–12,20–23]

A major challenge in producing larger glass parts using DIW has been preventing the formation of cracks in the green body caused by stresses generated during the consolidation process, as the organic components are volatilized at elevated temperatures.[24,25] Both the drying and binder burn-out stages of the heat treatment require careful control of the evaporation/pyrolysis rates. Along with controlling temperature ramp rates and appropriate dwell times, it is important to select a solvent with a boiling point well above room temperature to reduce or mitigate rapid post-printing drying. These problems are further exacerbated with increased size and high aspect ratios. As the critical dimension of the printed part increases, so does the time required for diffusion of the solvent to take place across the densifying solid matrix. For geometries with high aspect ratios, the stress distribution becomes increasingly anisotropic, leading to large scale warping and cracking. Hence, to date, indirect printing of glass using silica-loaded inks has generally been constrained to parts < 20 mm with no unsupported or high aspect ratio features.

For applications where simple monolithic shapes are desired, the rate of elastic recovery associated with stress relaxation as the particle network restructures is sufficiently high to maintain the deposited shape. However, when printing unsupported overhang features or high aspect ratio structures, the stresses often exceed the yield stress of the ink, leading to warping or collapse of printed features.[26] Combining UV-curing capability with DIW by incorporation of photosensitive acrylate monomers and photoinitiators to the inks increases the ink viscosity range, green strength, and geometric flexibility for DIW glass. The ability to cure print lines in place during printing enables improved self-support of the print which facilitates overhangs and high aspect ratio features.[13,27]

Here we present a formulation, printing method, and processing route that combines the advantages of in situ UV curing with the shear and the mixing capabilities of in-line active mixing to create optically transparent silica glass (**Figure 1**). Enhanced control of the setting rate by relying on applied UV intensity instead of solely elastic recovery enables expanded geometric freedom to print high aspect ratio structures and unsupported features. Incorporation of UV curing acrylates also improves the green strength of the printed part, which facilitates a 3× increase (volumetric increase of 45×) in the shapes that can be converted into crack-free glass. Finally, the introduction of active mixing to the DIW system both expands the ink viscosity range that can be printed by applying high shear during mixing and blends multiple ink formulations to create compositional gradients within the print. These advances combined make UV-DIW with active mixing an excellent method for creating geometrically and compositionally complex prints from at fine scales ≈10 mm to larger dimensions up to 44 mm.

2. Experimental Section

2.1. Ink Formulation

Inks for this study were formulated with varying proportions of two solvents: propylene carbonate (PC, Sigma–Aldrich) and tetraethylene glycol dimethyl ether (tetraglyme, TG, Sigma–Aldrich). Two types of SiO_2 nanoparticles, EH5 (CAB-O-SIL) with a d_{50} of 22 nm, and TT600 (Aerosil TT 600, Evonik) with a d_{50} of 70 nm were compared in this study. Ratios were kept constant between the solvents (PC or TG) and the monomers 2-hydroxyethyl acrylate (HEA, Sigma–Aldrich) and 1,6-hexanediol diacrylate (HDDA, Sigma–Aldrich), at a ratio of ≈2:1 solvent:monomers and 2.5:1 HEA:HDDA. The amount of photoinitiator, TPO-L (ethyl (2,4,6-trimethylbenzoyl) phenylphosphinate, Rahn USA Corp.), was adjusted to a vol% ratio of 86:1 to 43:1 monomer:TPO-L depending on the formulation (0.01 to 0.03 wt.% TPO-L when compared to monomer weight). When indicated, 5 vol% phenoxyethanol (PE, Sigma–Aldrich) was substituted for an equal vol% of solvent as a dispersant. Further formulation details can be found in **Table 1**. A planetary mixer (ARM-310, Thinky) was used to mix all inks at 2000 rpm for 30 s intervals until each ink was homogenous and transparent, on average requiring 5–8 mixing iterations depending on formulation. The ink containers were cooled in a water bath between mixing steps to minimize solvent evaporation and potential for thermal curing of the acrylates. When stored at low temperatures (≈4 °C), this ink remained printable, after repeating one mixing step, for up to two months. This is a reduced shelf life when compared to non-UV DIW inks or stereolithography inks which can be stable for considerably longer, because an inhibitor is not included. Therefore,

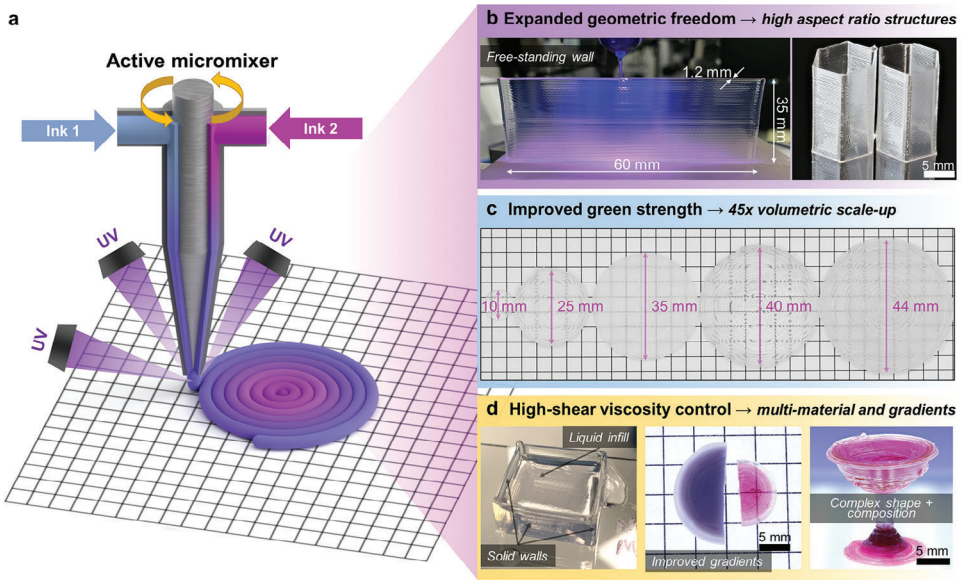

Figure 1. a) A schematic of the UV-assisted DIW setup equipped with an active micromixer. b) The UV curing capability enables printing of otherwise unstable structures, such as free-standing walls (left) and tall thin-walled objects (right). c) The addition of photo-curable polymers to the silica inks improves the resistance to cracking of the printed green body during heat treatment, allowing fabrication of larger glass parts than previously reported, such as disks measuring up to 44 mm in diameter and 3.5 mm thick. d) The rotation speed of the micromixer can be used to control the level of shear thinning applied to the ink, which, when coupled with UV curing, allows printing of materials with disparate viscoelastic properties (left), improved compositional gradients (center), and combinations of complex shapes and compositions (right).

storage at a low temperature slows the rate of polymerization during storage and extends the shelf life of the resin.[28] The resin will become unmixable after storage at room temperature for 7 days due to this uninhibited polymerization.

2.2. Rheology

Rheological characterization was conducted using an oscillatory rheometer (DHR-2, TA Instruments) with a UV curing attachment (TA Instruments) and external UV source (Omnicure S200) with a 365 nm filter. Parallel plates 20 mm in diameter were used for each measurement, the base plate being transparent quartz and the top plate being aluminum (TA Instruments, New Castle, DE). After loading into the fixture at a gap height of 200 µm, each ink was then allowed to relax under low strain conditions (0.01% strain, 1 Hz) for 20 min and the storage and loss moduli were recorded to measure the recovery time. After recovery, an oscillatory amplitude sweep was conducted from 0.01% strain to 100% strain to measure the yield stress of each ink. Finally, an additional 20 min of relaxation at 0.01% strain was used to measure the time for the storage modulus to exceed the loss modulus once more, or the recovery time, and was followed by performing a viscosity flow sweep between 0.01 and 100 s^{-1}. Additionally, on a separate sample the low stress oscillatory measurement was repeated, but UV light (365 nm) was applied through the quartz bottom geometry after 30 s of measurement. The time for the storage modulus to surpass the loss modulus was then recorded as the curing time.

Table 1. Formulation ranges, by volume, for the UV inks used in this study.

Component	Purpose	Density [g mL^{-1}]	Volume %
Fumed silica	Glass former	2.20	12–22
TG	Solvent	1.009	0–57.2
PC	Solvent	1.205	0–57.2
PE	Dispersant	1.100	0–5.5
HEA	Monoacrylate	1.011	19.0–19.9
HDDA	Diacrylate	1.029	7.5–7.9
TPO-L	Photoinitiator	1.146	0.32–0.77

2.3. Printing Process

A modified 4-axis setup (x-y-z and a rotary stage, Aerotech) was used for all sample printing. Ink was deposited by using two linear actuators to displace ink from a 30 cc syringe through PFA tubing and into the active mixing chamber before exiting the system through a stainless-steel nozzle (ID 250–1540 µm). Each sample was printed at room temperature on a porous aluminosilicate substrate plate (McMaster-Carr, Elmhurst, IL) while applying ≤ 1 mW cm^{-2} of UV intensity (365 nm filtered) via the light guides, as measured at the illuminated area on the substrate (Figure 1a). After printing, parts were cured in a UV box (XYZ Curing Chamber) at 18 mW cm^{-2} for 5 min and released from the substrate using a thin wire.

2.4. COMSOL Modeling

To determine shear rate and viscosity differences between the active mixer being engaged at 160 rpm and no active mixing occurring, COMSOL was used. A COMSOL model approximating the

mixing volume was generated using viscosity information from the appropriate ink. The model was of the cylindrical portion of the mixing body only, and mixing was approximated by setting the inner wall to spin at either 160 rpm (mixing) or 0 rpm (no mixing). The velocity profile and gap between the mixing body wall (outside of cylinder) and mixing shaft (inside of cylinder) were then used to calculate the shear rate as a function of location in the cross-section (Figure S1, Supporting Information). For the deposition nozzle, the flow rate and nozzle diameter were used to calculate the shear rate at the nozzle wall, where the shear rate will be the highest.

2.5. Thermal Processing

After the cured part was released from the substrate, all samples were dried on the porous aluminosilicate substrate to promote solvent evaporation from all sides, ramping at 0.1 °C min^{-1} to 100 °C. Printed and dried walls were then scanned using a profilometer (Keyence VR-3200, Illinois), and angles of bending were measured using the Keyence software. To remove the organic material from the prints, the following binder burn-out profile was used in a box furnace (Vulcan Muffle Furnace, Neytech): 0.1 °C min^{-1} ramp to 190 °C with a 12 h hold, 0.1 °C min^{-1} ramp to 250 °C with an 18 h hold, 0.1 °C min^{-1} ramp to 600 °C with a 12 h hold. These temperatures were determined via DSC data in Figure S2 (Supporting Information). Slow ramp rates and long dwell times at elevated temperatures are essential to ensure total volatilization of the organic components through the pore network of the green part, especially with larger prints. Residual carbon in the green part would become trapped as porosity closes during the sintering process and negatively impact the optical clarity of the glass.[9] After burn-out, samples were consolidated by ramping to 1400 °C at a rate of 10 °C min^{-1}, followed by an immediate furnace cooling phase. This is in contrast to previous work by LLNL, as a slow ramp and hold at 1200 °C produced opaque samples with the UV system (Figure S3, Supporting Information).[9,10]

3. Results and Discussion

The printability of inks in DIW is a function of the material rheology – typical inks are YSFs possessing fast elastic recovery times required to retain the shape of the extruded filament upon exiting the nozzle. The addition of a UV light source provides an additional level of control over the setting of the extruded shape by photocuring the material after it exits the nozzle. By adjusting the kinetics of the elastic recovery and the photopolymerization reaction, the UV-DIW print parameters can be optimized for a given material (**Figure 2**).

The concentration of photoinitiator (TPO-L) affects both the rheology and the reaction kinetics. Increasing the TPO-L content has an effect on the cure rate of the ink which is apparent only at lower intensities of applied UV light due to saturation of the crosslinking reaction rate. At 1 and 2 mW cm^{-2}, normalized cure time (the amount of time necessary for the storage modulus to exceed the loss modulus upon application of UV light (t_{cure}) divided by the recovery time of the ink (t_{rec})) decreases dramatically as TPO-L is initially increased from 0.32 to 0.40 vol%. Normalized cure time is used here to eliminate the differing recovery times of the inks from the cure time results, as inks with higher TPO-L contents were slower to recover. At TPO-L contents 0.40 vol% and higher, the curing behavior is nominally the same according to the standard deviation of the measurements, as is shown in Figure 2 with normalized cure time converging ≈2. Additionally, increasing the UV intensity to 4 mW cm^{-2} at these higher TPO-L concentrations does not offer any additional increases to the curing rate. This indicates that, while additional TPO-L can assist in dispersion of the silica particles, to maintain flexibility in the curing rate a low concentration of TPO-L, 0.32 vol%, is ideal.

TPO-L also acts to lower viscosity in this particle-filled ink. Doubling the TPO-L content from 0.32 to 0.64 vol% drops the viscosity at 0.01 s^{-1} by an order of magnitude from 1.08×10^5 Pa s to 1.2×10^4 Pa s (Figure S4, Supporting Information); however, at shear rates approaching 100 s^{-1}, the viscosities of all these inks converge, as each contains the same proportions of silica and organics. Molecular weight of the organic components and how the organic molecules interact with both particle surfaces and each other are major drivers of dispersion rheology, as they affect how particles move past one another as they are being sheared (**Figure 3**). Larger, higher molecular weight solvents with a high dipole moment, such as TG, will yield a higher viscosity dispersion due to increased hydrogen bonding compared to PC, which is a smaller molecule with a lower dipole moment. The higher propensity of TG to hydrogen bond, as well as the higher molecular weight, can also be inferred from the higher viscosity of neat TG, which is 3.84 mPa s at 20 °C, compared to the viscosity of neat PC, which is 2.76 mPa s at 20 °C. This difference is observed in 14 vol% silica UV inks (Figure S5, Supporting Information) at shear rates >3 s^{-1}, where the viscosity of the PC-based dispersion drops significantly below that of the TG-based dispersion. The PC-based ink displays a very dramatic shear thinning behavior, starting at similar viscosities to the TG-based ink (≈10^6 Pa s) at rest, but dropping to 20 Pa s or less ≈60 s^{-1}. This suggests that PC is not as effective at keeping the silica particles well-dispersed at low shear rates when compared to TG, as the viscosity of neat PC is lower than neat TG. Smaller, less polar PC molecules do not provide the electrosteric hinderance between particles that larger, more polar TG molecules do, and therefore allow the silica particles to agglomerate when not under higher shear rates. This agglomeration raises the apparent viscosity because agglomerates trap fluid between the particles and thus artificially lower the amount of solvent present in the suspension.[19,29–31]

Ink viscosity can also be lowered using surfactants, which stabilize particles and lower aggregation by decreasing interparticle attractions (Figure 3). PE was chosen as it is compatible with the other polar organic components of the ink and has no constituents that would leave a residue during burn-out.[2] The addition of PE to a 14 vol% silica TG ink system decreases the low-shear viscosity by an order of magnitude, and the high-shear viscosity is halved (Figure S6, Supporting Information). The optimal PE volume fraction for this ink was found to be 5.3 vol%, a fairly high concentration which is attributed to the high specific surface area of EH5.

Particle loading and particle size are well-known parameters for tuning rheology (Figure 3), and the use of nanoparticles makes the rheological response more sensitive to small changes

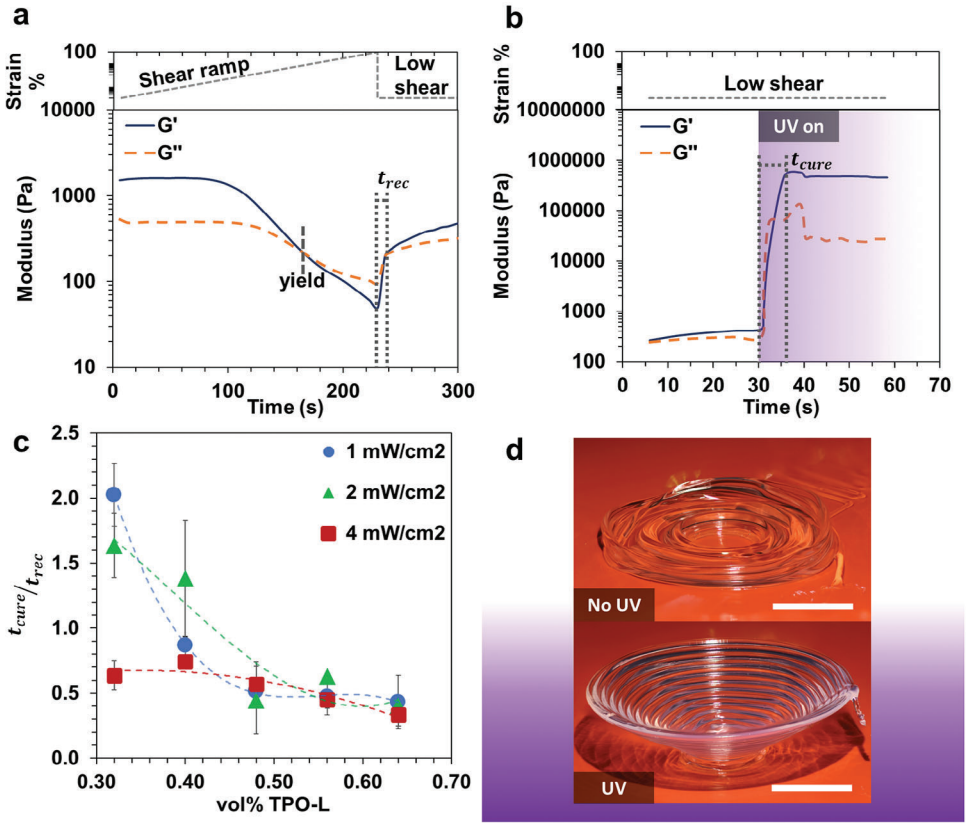

Figure 2. The process to evaluate rate of curing accounting for elastic recovery. a) Measurement of the yield stress and subsequent low-stress recovery, starting at 220 s, to obtain relaxation time for a given ink. b) Measurement cure time by applying oscillatory stress and exposing the ink to a UV source beginning at 30 s. c) Comparison between different TPO-L concentrations and the normalized curing time (t_{cure}/t_{rec}), dotted lines included to guide the eye and do not indicate any mathematical fit. d) The same ink without and with UV applied during printing, scale bar is 5 mm.

in particle loading. Increasing the silica content from 12 to 14 vol% raises the low-shear viscosity by an order of magnitude (from 10^4 to 10^5 Pa s). Further addition of silica to 18 vol% increased the viscosity to 3.55×10^6 Pa s (Figure S6, Supporting Information). These dramatic increases with relatively small silica additions are typical of a nanoparticle system, where the surface area to volume ratio is high and therefore leads to more surface interactions between particles, which raises the viscosity quickly compared to larger, lower surface area to volume particles. Overall, with the goal of increasing green part strength, particle loading was increased from 12 to 18 vol% by adjusting surfactant concentration, average particle size, and solvent composition.

Evaluation of warping is extremely important for scale-up considerations, as large, higher surface area prints will warp more than small, lower surface area prints. However, this is a challenging measurement to obtain even with simple geometries, as parts can warp and twist in various directions. To explore this, walls of various aspect ratios were printed and, after drying, scanned to determine the degree of warping when dried with the walls laying down on the substrate. Warping in different directions was approximated by measuring four angles of bending and adding those together for each sample (**Figure 4**). These summations were then compared across different aspect ratios and silica loadings to determine the effect of silica loading on how the ink behaves during drying, which was observed to be the step that most often resulted in cracking. For each ink formulation, the low aspect ratio parts warped the least during drying, as would be expected when comparing the surface stresses of drying to the relative volume of each part. Of the three silica loadings tested, at low aspect ratios the 18 vol% silica prints warped the least by a factor of 2. When the aspect ratio was increased, the degree of warping also increased for all ink formulations to fairly similar values. Warping behavior of higher aspect ratio geometries will require additional work to quantify effectively, as high aspect ratio prints displayed a large degree of curling and slanting which is not easily captured with this method. However, thorough understanding of warping and its complexity will be key to scale-up efforts. It is important to note that all prints in Figure 4 were processed to crack-free transparent glass.

Due to decreased warping during drying with increased solids loading, and work by Dudukovic et al. which demonstrated viscosity tuning with addition of TT600 silica to a dispersion of EH5 silica,[11] TT600 silica was added to replace 2/3 of the EH5 content in the ink by weight to increase the processable print size. As the proportion of TT600 silica increased, solids loading of up to 22 vol% was possible in the DIW ink while maintaining a workable viscosity and shorter ink mixing time (≈10 min). This is due to the much lower specific surface area of TT600 silica when compared to EH5 silica, at 200 and 380 $m^2\ g^{-1}$ respectively, as well as

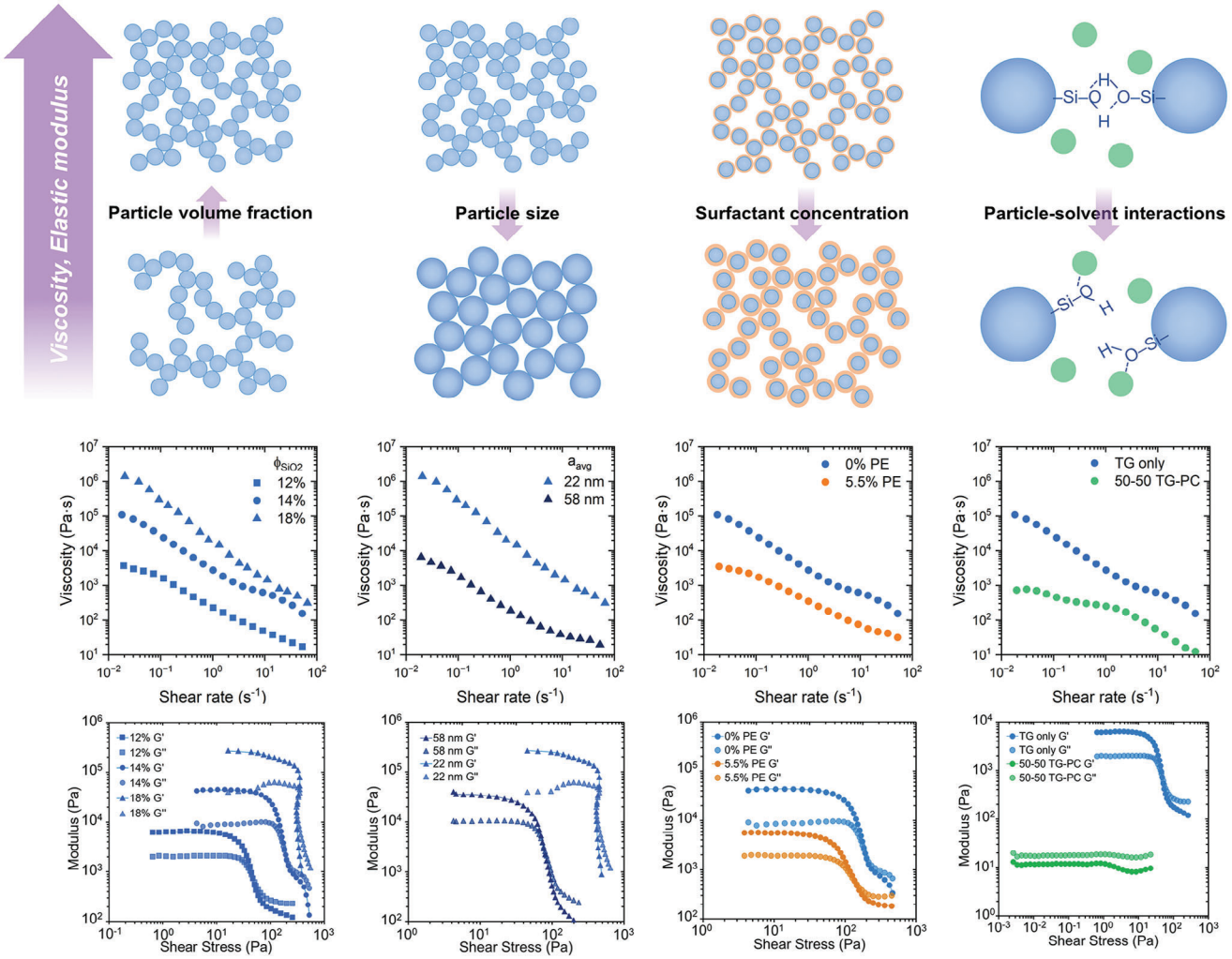

Figure 3. Illustration of the effects of ink formulation on rheological properties. Top row plots: shear rate-dependent viscosity; bottom row plots: storage (G′) and loss (G″) shear moduli as a function of oscillation strain.

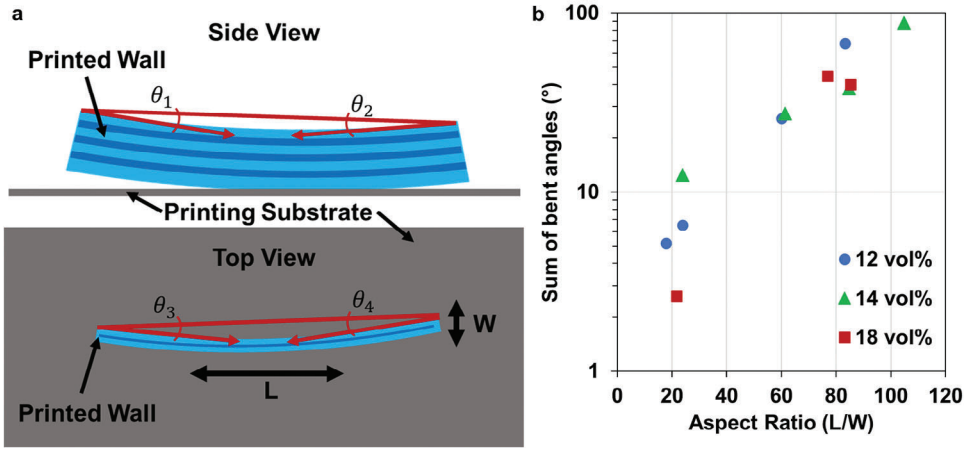

Figure 4. A) A schematic showing the warping angles measured for each sample. B) The sum of bend angles parallel and perpendicular to the print direction in rectangular samples, as measured by high resolution Keyence scanning, versus aspect ratio for inks with 12, 14, and 18 vol% loading of silica.

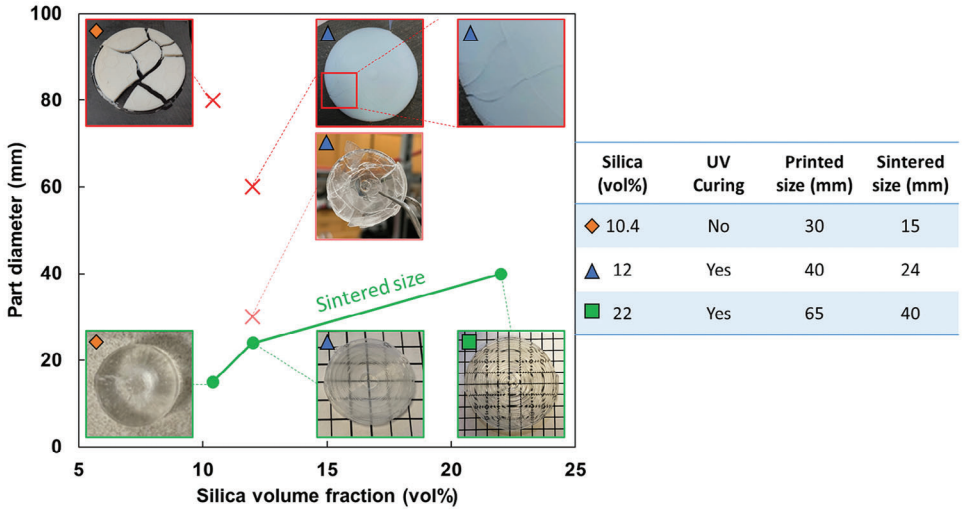

Silica (vol%)	UV Curing	Printed size (mm)	Sintered size (mm)
◆ 10.4	No	30	15
▲ 12	Yes	40	24
■ 22	Yes	65	40

Figure 5. Comparisons of dried and sintered silica glass disks produced with an ink with no acrylates and 10.4 vol% silica, an acrylate containing UV ink with 12 vol% EH5 silica, and an acrylate containing UV ink with 22 vol% EH5 and TT600 silica in a 1:2 ratio.

a more bimodal particle size distribution, since the d_{50} for TT600 and EH5 are 70 and 22 nm. Inks with some or all of the EH5 replaced by TT600 would therefore be expected to be lower in viscosity at the same particle loadings.

Increasing the solids content to 22 vol% increased the processable part size from 15 to 44 mm in diameter for 3 mm thick printed disks, as measured after processing to fully dense silica glass (**Figure 5**). While walls were not printed with the 22 vol% ink, based on the trend in low aspect ratio (≈20) walls, the low aspect ratio disks shown here should exhibit decreasing degrees of warping as the silica content increases from 10.4 to 22 vol%. Additionally, the linear shrinkage from printed part to sintered glass changes from 50% with the 10.4 vol% silica ink to 30% for the 22 vol% silica ink (Figure 5). A part that experiences less warping and shrinkage during thermal processing will also experience less stress, which improves the rate of survival to uncracked glass parts. In addition to decreased warpage, one can expect that as the volume loading of silica particles in the acrylic matrix increases, the failure strength of the green part will also increase. We attribute these two factors to the dramatic improvement in print robustness and final glass print quality shown in Figure 5, where ≈50% of non-UV prints with 10.4 vol% silica survive thermal processing with no cracking, compared to 100% of prints surviving with the 22 vol% silica UV prints.

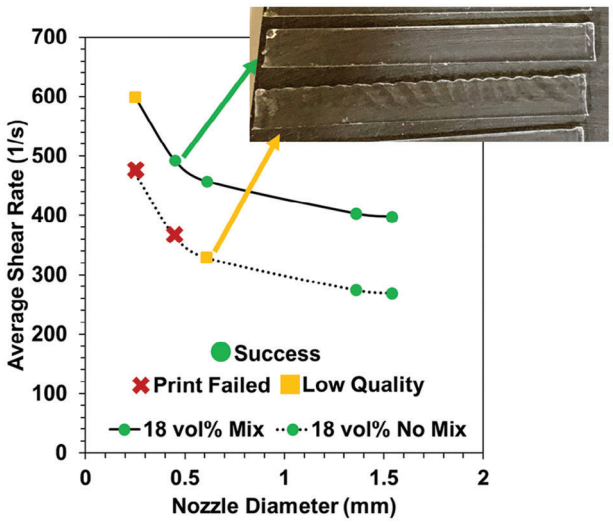

Figure 6. Average shear rate during mixing versus nozzle diameter with the active mixer turned on or off. Success or failure of a 2-filament wall print is indicated on each data point for the 18 vol% EH5, 0.30 vol% TPO-L, 4.6 vol% phenoxyethanol ink, with examples of a successful (top) and low-quality (bottom) print shown for two data points.

Printing of high viscosity inks through small (sub-mm) nozzles often faces challenges of clogging, which occurs when extremely high pressures are needed to facilitate extrusion. These difficulties can be overcome using an active micromixing nozzle.[12,32] The high shear fields imparted in the mixer lower the viscosity of inks as they are extruded, which also enables printing with smaller nozzle sizes. Figure 5 shows average shear rate versus nozzle diameter for the 18 vol% EH5, 0.32 vol% TPO-L, 4.6 vol% phenoxyethanol ink. Shear rate was approximated by averaging the highest shear rate ($\dot{\gamma}$) moving through the nozzle at any point in the diameter (d) at a flow rate of δv, calculated by $\dot{\gamma} = \delta v/d$ and the maximum shear rate generated by the active mixer running at 160 rpm, as simulated from COMSOL models (Figure S1, Supporting Information). Because active mixing significantly lowers the viscosity of the inks, by increasing the magnitude of shear rate the inks experience, 2-filament walls with straight sides were able to be printed from nozzles as small as 0.41 mm in diameter with the mixer. A low viscosity at the nozzle exit allows the filaments to knit together to form a coherent wall,[33] and also mitigates clogging when small diameter nozzles are used. In contrast, without the mixer, the practical nozzle size limit with the 18 vol% EH5 ink was ≈0.61 mm in diameter, which printed as a coherent wall but displayed print defects such as filaments laterally bending as they exit the nozzle due to the short recovery time of the ink. This causes the

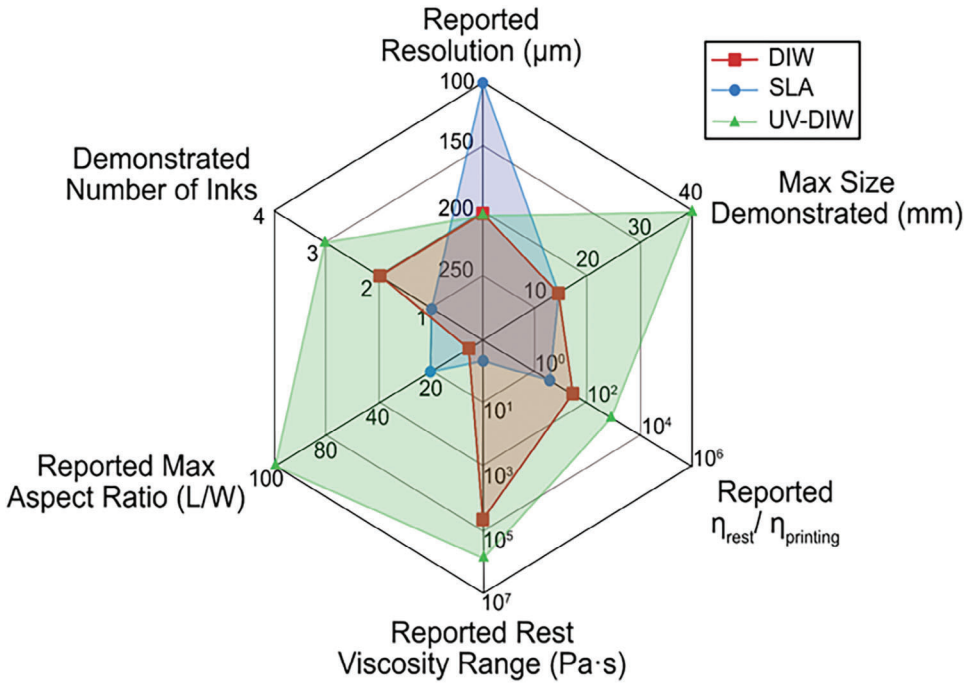

Figure 7. A radar plot showing values reported in the literature for stereolithography,[2–4] DIW,[9–12,21] and UV-DIW (this work) of optically transparent glasses, where number of inks is set by inks used in the same print, rest viscosity is defined as the viscosity at 0.01 s^{-1} and printing viscosity is determined from shear rate in a given printing process.

filament to stop flowing as it exits the nozzle and therefore it does not flatten as it contacts the layer underneath. Additionally, depositing a stiff filament onto a partially cured wall can push the layers beneath it out of place, causing the wall to slant or waves to appear in the wall structure (**Figure 6**). Active mixing during printing also introduces the ability to print gradients of different ink compositions.[12] This capability was used to introduce gold nanoparticle gradients which visibly alter the glass to illustrate gradients and to print three inks of different viscosities to flood a stiff outer wall with two low viscosity inks, one doped and one undoped, to ensure a void-free gradient composition bulk (Figure 1d).

To ensure the glass prints would be suitable for transmissive or reflective optic applications, some solid disks were polished so the faces of the disk were smooth and parallel to a surface roughness of 1–2 nm. After polishing, with no post-polish annealing, the samples were imaged under a cross polarizer to detect any polishing stresses, in which no stresses were visible (Figure S7a, Supporting Information). A printed 25 mm × 4 mm disk was polished to the same specifications and the optical homogeneity was measured on the center 18 mm with a 6″ Zygo Verifire PSI interferometer from three different orientations three times each. After accounting for system noise from the measurement being done in air, the peak-to-valley (PV) refractive index homogeneity of the disk was measured to be 14.57 ppm with a root mean square of 2.16 ppm. This value can be improved by perfecting the tool path to ensure total infill, as print lines can be seen in the homogeneity measurement (Figure S7b,c, Supporting Information). However, these values still fall within acceptable optical glass properties.[10] Due to the lack of polishing stresses and relatively homogenous refractive index, it can be hypothesized that these prints would have sufficient mechanical strength for applications in optics.

4. Summary

This work has highlighted the importance of ink formulation, printing conditions, and post-processing to printing high quality solid glass geometries up to 44 mm in diameter and 3 mm thick. Key aspects include: introduction of a UV-active component to the ink to enable overhangs and high aspect ratio prints, implementing active mixing to lower the printing viscosity to print more viscous inks, increasing the green strength of the print with increased solids loading and UV-curing acrylates, and decreasing drying warpage and sintering shrinkage by increasing silica content in the ink. In addition to increasing the processable size by ≈3×, adjusting the ink formulation and introducing UV curing to the printing process facilitated the printing and processing of complex, high aspect ratio, and self-supporting multimaterial glass geometries. These advances set the stage for UV-DIW glass to be applied in various custom optic applications that were previously too large or too complex to achieve with DIW, such as camera lenses or reinforced mirrors (**Figure 7**).

Supporting Information

Supporting Information is available from the Wiley Online Library or from the author.

Acknowledgements

This manuscript has been authored by Lawrence Livermore National Security, LLC under Contract No. DE-AC52-07NA2-7344 with the US.

Conflict of Interest

The authors declare no conflict of interest.

Data Availability Statement

The data for this work is available upon request and subject to review due to being generated by Lawrence Livermore National Security, LLC under Contract No. DE-AC52-07NA2-7344 with the US. Department of Energy.

Keywords

additive manufacturing, direct ink write, glass, optics, rheology, UV curing

Received: August 6, 2024
Revised: October 22, 2024
Published online:

[1] J. Luo, J. M. Hostetler, L. Gilbert, J. T. Goldstein, A. M. Urbas, D. A. Bristow, R. G. Landers, E. C. Kinzel, *Opt. Eng.* **2018**, *57*, 1.
[2] F. Kotz, K. Arnold, W. Bauer, D. Schild, N. Keller, K. Sachsenheimer, T. M. Nargang, C. Richter, D. Helmer, B. E. Rapp, *Nature* **2017**, *544*, 337.
[3] C. Liu, B. Qian, R. Ni, X. Liu, J. Qiu, *RSC Adv.* **2018**, *8*, 31564.
[4] P. Cai, L. Guo, H. Wang, J. Li, J. Li, Y. Qiu, Q. Zhang, Q. Lue, *Ceram. Int.* **2020**, *46*, 16833.
[5] J. T. Toombs, M. Luitz, C. C. Cook, S. Jenne, C. C. Li, B. E. Rapp, F. Kotz-Helmer, H. K. Taylor, *Science* **2022**, *376*, 308.
[6] L. A. Myers, J. J. Schwartz, M. P. De Beer, R. L. Walton, D. H. Porcincula, *J. Polym. Sci.* **2024**, *62*, 2683.
[7] F. Kotz, A. S. Quick, P. Risch, T. Martin, T. Hoose, M. Thiel, D. Helmer, B. E. Rapp, *Adv. Mater.* **2021**, *33*, 2006341.
[8] M. Li, L. Yue, A. C. Rajan, *Sci. Adv.* **2023**, *9*, eadh7828.
[9] D. T. Nguyen, C. Meyers, T. D. Yee, N. A. Dudukovic, J. F. Destino, C. Zhu, E. B. Duoss, T. F. Baumann, T. Suratwala, J. E. Smay, R. Dylla-Spears, *Adv. Mater.* **2017**, *29*, 1701181.
[10] J. F. Destino, N. A. Dudukovic, M. A. Johnson, D. T. Nguyen, T. D. Lee, G. C. Egan, A. M. Sawvel, W. A. Steele, T. F. Baumann, E. B. Duoss, T. Suratwala, R. J. Dylla-Spears, *Adv. Mater. Technol.* **2018**, *3*.
[11] N. A. Dudukovic, L. L. Wong, D. T. Nguyen, J. F. Destino, T. D. Yee, F. J. Ryerson, T. Suratwala, E. B. Duoss, R. Dylla-Spears, *ACS Appl. Nano Mater.* **2018**, *1*, 4038.
[12] R. J. Dylla-Spears, T. D. Yee, K. Sasan, D. T. Nguyen, N. A. Dudukovic, J. M. Ortega, M. A. Johnson, O. D. Herrera, F. J. Ryerson, L. L. Wong, *Sci. Adv.* **2020**, *6*, eabc7429.
[13] A. De Marzi, G. Giometti, J. Erler, P. Colombo, G. Franchin, *Addit. Manuf.* **2022**, *54*, 102727.
[14] L. Rich, D. Crowe, *SPIE* **1995**, *2543*, 236.
[15] M. T. Jacoby, E. E. Montgomery, A. J. Fontini, W. A., Goodman, *Proc. SPIE* **1999**, *3786*, 12363826.
[16] J. Cesarano, Robocasting of Ceramics and Composites Using Fine Particle Suspensions, Sandia National Laboratory, Albuquerque, New Mexico **1999**.
[17] J. Cesarano, *Mater. Res. Soc. Sympos. – Proc.* **1999**, *542*, 133.
[18] M. A. S. R. Saadi, A. A. Maguire, N. T. Pottackal, M. S. H. Thakur, M. M. Ikram, A. J. Hart, P. M. Ajayan, M. M. Rahman, *Adv. Mater.* **2022**, *34*, 57.
[19] M. Subbanna, S. G. MalghanS, *Chem. Eng. Sci.* **1998**, *53*, 3073.
[20] J. Ha, K. Sasan, T. D. Yee, A. P. Lange, D. T. Nguyen, N. Dudukovic, R. Dylla-Spears, *Adv. Photon. Res.* **2022**, *3*, 2200017.
[21] K. Sasan, A. Lange, T. D. Yee, N. Dudukovic, D. T. Nguyen, M. A. Johnson, O. D. Herrera, J. H. Yoo, A. M. Sawvel, M. E. Ellis, C. M. Mah, R. Ryerson, L. L. Wong, T. Suratwala, J. F. Destino, R. Dylla-Spears, *ACS Appl. Mater. Interfaces* **2020**, *12*, 9b21136.
[22] I. Cooperstein, E. Shukrun, O. Press, A. Kamyshny, S. Magdassi, *ACS Appl. Mater. Interfaces* **2018**, *10*, 18879.
[23] J. Wang, B. Zheng, P. Wang, *J. Non-Cryst. Solids* **2020**, *550*, 129362.
[24] T. J. Garino, H. K. Bowen, *Commun. Am. Ceram. Soc.* **1987**, *70*, C315.
[25] P. Calvert, M. Cima, *J. Am. Ceram. Soc.* **1990**, *73*, 575.
[26] J. B. Kim, H. Y. Lee, C. Chae, S. Y. Lee, S. H. Kim, *Adv. Mater.* **2023**, *36*, 2307917.
[27] B. M. Howell, C. C. Cook, M. D. Grapes, K. Dubbin, E. L. Robertson, J. D. Sain, K. T. Sullivan, E. B. Duoss, E. V. Bukovsky, *Adv. Mater. Technol.* **2022**, *7*, 7.
[28] A. W. Meyer, *Ind. Eng. Chem.* **1949**, *41*, 1570.
[29] J. E. Smay, J. C. III, J. A. Lewis, *Langmuir* **2002**, *18*, 5429.
[30] Y. K. Leong, D. V. Boger, D. Parris, *J. Rheol.* **1991**, *35*, 149.
[31] Z. Zhou, M. J. Solomon, P. J. Scales, D. V. Boger, *J. Rheol.* **1999**, *43*, 651.
[32] A. M. Golobic, M. D. Durban, S. E. Fisher, *Adv. Eng. Mater.* **2019**, *21*, 201900147.
[33] N. A. Dudukovic, M. E. Ellis, M. M. Foster, R. L. Walton, D. T. Nguyen, B. Giera, R. Dylla-Spears, *Rheol. Acta* **2022**, *61*, 773.

